Available online at www.sciencedirect.com
ScienceDirect
Earth and Planetary Science Letters 257 (2007) 622–634
EPSL
www.elsevier.com/locate/epsl

Impacts of tectonic changes on the reorganization of the Cenozoic paleoclimatic patterns in China

Zhang Zhongshi [a,b,*], Wang Huijun [a], Guo Zhengtang [b], Jiang Dabang [a]

[a] *Nansen-Zhu International Research Center, Institute of Atmospheric Physics, Chinese Academy of Sciences, Beijing, 100029, China*
[b] *Institute of Geology and Geophysics, Chinese Academy of Sciences, Beijing, 100029, China*

Received 16 October 2006; received in revised form 1 March 2007; accepted 13 March 2007
Available online 20 March 2007
Editor: M.L. Delaney

Abstract

Geologic studies have illustrated that the planetary-wind-dominant climate in the Paleogene is changed into the monsoon-dominant one near the Oligocene/Miocene boundary in China. The evolution is marked by the changes of regional aridity/humidity contrasts. The contrasts occur between the south and the north part of China in the Eocene, and then between East China and Central Asia near the Oligocene/Miocene boundary, indicating the onset of monsoon-dominant climate in China. The impacts of the Himalaya–Tibetan plateau uplift and/or the Paratethys Sea retreat on the Asian monsoon have been well demonstrated. However, whether or not other factors have affected the above reorganization of paleoclimatic patterns remains a question to be addressed. Additional factors that should be addressed at least include the Indian Peninsular drift, the South China Sea expansion and the East China Sea transgression. Here we use the IAP-AGCM to explore their roles in the above paleoclimatic evolution. Our experiments demonstrate that the South China Sea expansion is another major forcing, in addition to the important roles of the Paratethys retreat and the Himalaya–Tibetan plateau uplift. On the contrary the impacts of the Indian Peninsular drift and the East China Sea transgression are relatively subordinate. The Himalaya–Tibetan plateau uplift plays a crucial role in the magnification of the aridity/humidity contrasts between the south and the north part of China. The Paratethys retreat, the Himalaya–Tibetan plateau uplift and the South China Sea expansion coact to cause the formation of the aridity/humidity contrasts between East China and Central Asia. The retreat and the uplift favor the dynamic condition, and the expansion provides the water vapor condition for the monsoon-dominant climate in China.

Keywords: tectonic movements; East Asian monsoon climate; Oligocene/Miocene boundary

1. Introduction

The East Asian monsoon dominates the basic modern climatic pattern in China [1]. The winter winds bring cold and dry air from Central Asia, and the summer winds bring warm and moister air from the tropical oceans, while a large extent of desert distributes in Central Asia.

Such a monsoon-dominant climate is formed near the Paleogene/Neogene boundary (also the Oligocene/Miocene boundary) [2–6], whereas the paleoclimate in the Paleogene is still dominated by the planetary wind system, with a zonal arid band extending from East

* Corresponding author. Nansen-Zhu International Research Center, Institute of Atmospheric Physics, Chinese Academy of Sciences, Beijing, 100029, China.
E-mail address: zhongshizhang@mail.iggcas.ac.cn (Z. Zhongshi).

0012-821X/$ - see front matter © 2007 Elsevier B.V. All rights reserved.
doi:10.1016/j.epsl.2007.03.024

China to Central Asia (Fig. 1). The above paleoclimatic evolution is marked by the two-step changes of the regional aridity/humidity contrasts. The contrasts between the south part and the north part of China (hereafter referred as the south–north contrasts) are firstly magnified in the Eocene. Subsequently, the contrasts between Central Asia and East China (hereafter referred as the east–west contrasts) are intensified near the Oligocene/Miocene boundary, indicating the onset of the monsoon climate in China.

The mechanisms of the monsoon climate have been subject to scrutiny by scientists. The classical theory that the land–sea thermal contrast is the key element to the monsoon phenomena (e.g., [7]) seems too simple to explain the formation of the East Asian monsoon, because of the existence of the land–sea thermal contrast without the East Asian monsoon system in the Paleogene [2–6]. A later theory invokes the seasonal movement of planetary wind as the main cause of monsoon (e.g., [8]). The theory can reasonably explain the essence of the tropical monsoon, but can not fully account for the East Asian monsoon, a complex of the tropical and the subtropical monsoon (e.g., [9]). Subsequently, recent numerical experiments (e.g., [10–15]) address the impacts of the Himalaya–Tibetan plateau uplift on the intensification of Asian monsoon and the Asian inland aridity. Several other studies [16–19] emphasize the important role of the Paratethys retreat.

In the Cenozoic, the large-scale reorganizations of the Asian land-sea distributions also include the South China Sea expansion, the Indian Peninsular drift and the East China Sea transgression. Previous geologic research (e.g., [20,21]) has pointed out the possible impacts of the South China Sea expansion on the monsoon climate over East Asia. Geologists are also aware of the potential influences of the Indian Peninsular drift and the East China Sea transgression on Chinese paleoclimate (e.g., Y.C. Lu, 2005, personal communication). However, the impacts of these three factors on the above paleoclimatic evolution have not yet been addressed from the modeling point of view. In the present study, we use the IAP-AGCM to examine the impacts of the above five tectonic factors, and explore the relationship between the Cenozoic tectonic movements and the paleoclimatic evolution in China.

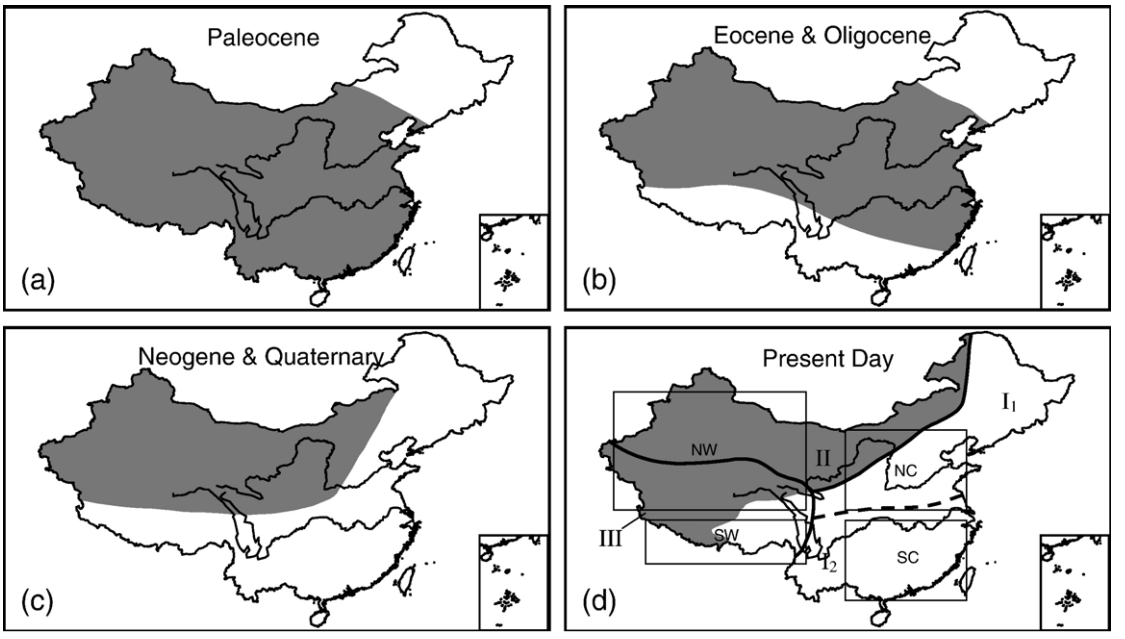

Fig. 1. Paleoclimatic evolution in China, (a) for the Paleocene, (b) for the Eocene to Oligocene and (c) for the Neogene to Quaternary. The shaded areas are arid/semiarid regions (Modified after Zhang and Guo [6]). In the present day (d) the whole China can be plotted into three basic regions [1], I the monsoon regions (I1 subhumid regions and I2 humid regions), II the arid/semiarid interiors and III the Himalaya–Tibetan plateau. Arid and semiarid regions with annual precipitation less than 400mm/y are shaded. According to the modern Chinese physical geography, four sub-regions are selected to diagnose the climatic evolution in the text, the Yangtze River valley and the area south of it (22°–30° N, 105°–120° E, denoted SC), the Yellow River valley (34°–42° N, 105°–120° E, denoted NC), North Tibet and Central Asia (34°–46° N, 75°–100° E, denoted NW), Himalaya and South Tibet (26°–30° N, 80°–100° E, denoted SW). SC and NC together are called East China. SC and SW together are titled the south part of China, and correspondingly NC and NW are named the north part of China.

2. Model and experimental design

The IAP-AGCM, designed and developed by the Institute of Atmospheric Physics, Chinese Academy of Sciences, is a global grid point model with 5°×4° (longitude by latitude) horizontal resolution, 9 unequally spaced levels in the vertical and the upper model boundary at 10 hPa. A comparison of the modern climate among the outputs of the IAP-AGCM, those of other models (CCC-II, GFHI, UKHI) and observations has illustrated that the model can realistically simulate the Asian monsoon (e.g., [23], Supplementary materials). The annual precipitation over the East Asian monsoon region, which is the most difficult to be accurately reproduced by models, is realistically simulated by the IAP-AGCM. The spatial correlation coefficient of precipitation is 0.80 between the simulations and the observations in the domain of 70–140° E and 15–60° N, and the root mean square error reaches 1.18 mm/day, which is partly due to the discrepancies (1–2 mm/day) presented over the Himalaya–Tibetan plateau [23]. The model also produces slightly more precipitation over the north part of China [22]. The model has been used in the simulations of paleoclimate (e.g., [18,19,23–26]). Detailed descriptions of the model can be found in Zhang [27], Liang [28] and Bi [22]. The performance of the model is demonstrated and discussed in Jiang et al. [23,24], Zhang et al. [18,19] and Ju et al. [25].

We focus on the large-scale reorganization of climatic patterns reflected by the changes of regional aridity/humidity contrasts, and only consider the coarse changes of topography and land–sea distributions, including 1) the uplift of the Himalaya–Tibetan plateau, 2) the shrinkage of the Paratethys Sea, 3) the expansion of the South China Sea, 4) the transgression of the East China Sea and 5) the north drift of the Indian Peninsula. Although the detailed changes of these above five factors are still under debate, such as the time and the height of the Himalaya–Tibetan plateau uplift, based on a large collection of geologic studies [2,20,29–49], a general picture that has emerged includes the following three assumptive but most likely scenarios. 1) When the Eurasian continent is divided by the Paratethys, neither the Himalaya–Tibetan plateau, nor the Indian peninsula and the present Chinese marginal sea exist in Asia [2,29]. 2) At the beginning of Indo-Asian collision, the Indian Peninsula takes its present location (e.g., [30]), the Himalaya–Tibetan plateau is low (e.g., [31,32]), the Chinese marginal sea is small [20,33] and the Paratethys is separated from the Arctic [34]. 3) The further Indo-Asian collision in the early Neogene leads to the larger South China Sea [20,33] and the accelerated Himalaya–Tibetan Plateau uplift [35]. The mountainous Himalaya–Tibetan plateau is on average higher than 1500 m (e.g., [36–41]) with the south part close to present height [42–45]. The Paratethys [46–48] and the East China Sea [49] are still minimal.

According to the above picture, two topography conditions (the middle and the low topography), three Paratethys Sea conditions (the large, the middle and the small Paratethys), two South China Sea conditions (the small and the absent South China Sea), two East China Sea conditions (the small and the absent East China Sea) and the absent Indian peninsula condition are designed (Fig. 2 a to k). Another three composite conditions are also designed to represent the above three scenarios (Fig. 2 l to n). In the following sections, the change in the lower boundary conditions from the Scenario I to the Scenario II is named the first stage of paleogeographic evolution, and the change from the Scenario II to the Scenario III is correspondingly called the second stage.

We do not evaluate the impacts of other potentially important climatic, tectonic or biotic events, for instance the development of north hemisphere ice-sheets [50,51], the Indonesian Seaway closing (e.g., [52]) or the C4 plants expansion (e.g., [53,54]), and also do not consider the changes of Earth orbital parameters, atmospheric CO_2 concentration. The Earth orbital parameters and vegetation use conditions of today [21]. The atmospheric CO_2 concentration is set to 345 ppmv (1975–1985 range is about 330 to 345 ppmv; [55]) in all experiments. The above two-step paleoclimatic evolution mainly involves the geologic course of the Eocene, the Oligocene and the Miocene [2–6]. These three periods are much warmer than the present (e.g., [50]). Unfortunately, no SSTs and ice-sheet reconstructions are available for these three periods. SSTs and ice-sheets data of the Middle Pliocene (also a warmer period than the present) [56] are used in all experiments. The SSTs are available for February and August only. Sinusoidal variation with extremes in February and August is used to get monthly varying SSTs. Additional sea points due to sea opening are prescribed the same SSTs as the neighboring sea point(s) at the same latitude. Additional land points due to sea closing are also prescribed the same topography and vegetation as the neighboring land point(s) at the same latitude.

One control run (Fig. 2a), ten sensitivity experiments (Fig. 2b–k) and three scenario experiments (Fig. 2l–n) are performed based on the above boundary conditions. All experiments are run for 12 years. The

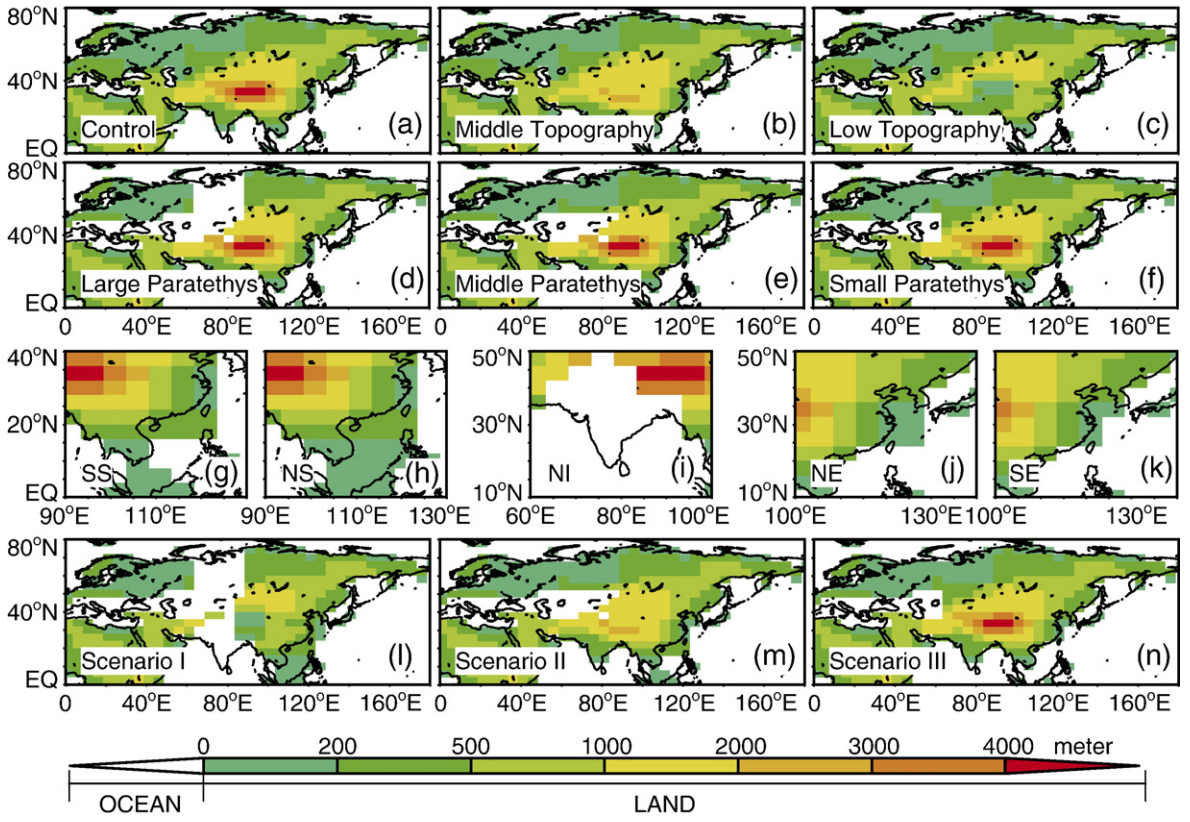

Fig. 2. Boundary conditions (a) for the control run, (b–k) for the sensitivity experiments, and (l–n) for the scenario experiments. The names of sensitivity experiments are the same as those of boundary conditions used. The control run (a) uses the present land–sea distribution and the topography with the Himalaya–Tibetan plateau having an average height of 3000 m. The Himalaya–Tibetan plateau is changed to averagely 1500 m high with maximum height 2800 m in the middle topography experiment (b), and there is no Himalaya–Tibetan plateau and the East Asia terrain is smooth without high mountains in the low topography experiment (c). Only topography is changed without altering the land–sea distributions in the above two topography experiments. The Paratethys Sea connects with the Arctic in the large Paratethys Sea experiment (d), retreats to the south part of West Siberia in the middle Paratethys Sea experiment (e), and then goes to the Turan Plate and Caspian areas in the small Paratethys Sea experiment (f). 3/5 of the South China Sea is changed to land in the small South China Sea (SS) experiment (g), and the whole South China Sea is substituted by land in the absent South China Sea (NS) experiment (h). The Indian peninsula is replaced by sea in the absent Indian Peninsula (NI) experiment (i). The whole East China Sea is turned to land in the absent East China Sea (NE) xperiment (j), and the half of the East China Sea is displaced by land in the small East China Sea (SE) experiment (k). Only the land–sea distributions are changed in the experiments from (d) to (k). The low topography, the large Paratethys, the absent Indian Peninsular, the absent South China Sea and the absent East China Sea conditions are aggregated in the Scenario I experiment (l). The middle topography, the middle Paratethys Sea, the small South China Sea and the small East China Sea conditions are assembled in the Scenario II experiment (m). The small Paratethys and the small East China Sea conditions are combined in the Scenario III experiment (n).

results reported here are ensemble averages for the last 10 years.

3. Analysis method

Two ratios are defined to describe the large-scale changes of the climatic patterns. M/I is the ratio of the regionally averaged precipitation over East China to that over North Tibet and Central Asia, and is hence indicative of the east–west aridity/humidity contrasts. For example, more precipitation over East China and less over North Tibet and Central Asia will lead to an increased M/I value, which indicates the intensification of the east–west contrasts and the East Asian monsoon climate. On the contrary, a decreased M/I ratio indicates a weakened monsoon climate. S/N is the ratio of the regionally averaged precipitation over the south part to that over the north part of China, and is indicative of south–north aridity/humidity contrasts.

The Static Normalized Seasonality (SNS, [57,58]) index describes the main characteristic of monsoon that the seasonal prevailing wind direction has a

significant seasonal change. It is used to measure the intensity of the monsoon and delimit the geographic distributions of the global monsoon systems.

$$\mathrm{SNS} = \frac{||F_1 - F_7||}{||\bar{F}||} - 2,$$

in which F_1 and F_7 are respectively the January and the July climatological wind vectors, and $\bar{F}$ is the annual average climatological wind vector. The norm $||A||$ is defined as $||A|| = (\int\int |A|^2 dS)^{0.5}$ where S denotes the domain of integration. Li and Zeng [58] have presented a detailed introduction for the calculations at a point. The SNS index based on the 850 hPa winds is calculated to explore the spatial development of monsoon areas over East China.

Sea level pressure, 850 hPa winds and other variables are also used in the analyses. Statistical significance is assessed by the student *t*-test (95% level) applied to differences between every two experiments. The standard deviation and degrees of freedom are based on the averages of the 10 individual years.

4. Results of sensitivity experiments

4.1. Topography and Paratethys Sea

Previous studies [10–14] have demonstrated that the Himalaya–Tibetan plateau uplift intensifies the monsoon circulations, increases precipitation over East China and decreases precipitation over Central Asia. Our earlier studies [18,19] have also illustrated that the Paratethys retreat from the south part of West Siberia to the Turan plate is the most important period for the intensification of the East Asian monsoon. The retreat in this period also induces the remarkable shifts to more precipitation over East China and less over Central Asia.

Our sensitivity experiments support the earlier studies [10–19]. Lowering topography results in the reduced S/N and M/I ratios and SNS values (Table 1), indicating that the strong impacts of the Himalaya–Tibetan plateau uplift on the intensification of the East Asian monsoon and the magnification of the regional aridity/humidity contrasts (south–north and east–west contrasts). The Paratethys retreat also enhances the east–west aridity/humidity contrasts. The most prominent changes of the M/I ratio (Table 1) occur when the Paratethys retreats from the south part of West Siberia (the middle condition) to the Turan plate and Caspian areas (the small condition).

4.2. South China Sea

The closing of the South China Sea markedly reduces precipitation over East China (Fig. 3a and b). The sea closing to a small size causes 24.52%, 7.43% and 12.07% decreased precipitation respectively over the Yangtze River valley and the area south of it, the Yellow River valley, and Himalaya and South Tibet, as well as 8.03% increased precipitation over North Tibet and Central Asia. These precipitation changes produce a 0.68 reduction in M/I and a 0.56 decrease in S/N. The replacement of the whole South China Sea by land causes a decrease of 42.11%, 8.24% and 16.32% in precipitation respectively over the Yangtze River valley and the area south of it, the Yellow River valley and Himalaya and South Tibet, and a 7.17% increase in precipitation over North Tibet and Central Asia. These precipitation changes result in the reductions ΔM/I of 0.96 and ΔS/N of 0.86 relative to the control run.

The closing of the sea also changes the land–sea thermal contrasts and leads to the reorganizations of pressure structure, which cause the wind anomalies (Fig. 3c to f). However, the anomalies in 850 hPa winds and the variations of SNS values appear to be less obvious than the changes in the regional aridity/humidity contrasts. This reflects the less important impacts of the South China Sea forcing on the monsoon circulation and wind seasonality.

4.3. Indian Peninsular

The removal of the Indian Peninsular leads to an increase of 12.37%, 2.45% and 25.16% in precipitation respectively over the Yangtze River valley and the area south of it, the Yellow River valley and North Tibet and Central Asia, plus a 3.65% decrease in precipitation over Himalaya and South Tibet. These changes in precipitation produce a ΔM/I of 0.36 and a ΔS/N of 0.25 less than the control (Table 1). The removal also causes a reduction in SNS of 62.33% over East China. The change in SNS values is much larger than the variations of the M/I and S/N ratios, indicating the major impact of the Indian Peninsular drift on the atmospheric circulations and the wind seasonality over East Asia.

4.4. East China Sea

The closing East China Sea to the small size only produces a 0.10 reduction in M/I and a 0.20 increase in S/N compared to the control run. The replacement of the whole sea by land causes a precipitation decrease of 9.33%, 32.80% and 0.24% respectively over the Yangtze River

Table 1
Chinese climate responses to different boundary conditions

	ΔP[a] (%)				ΔM/I[f]	ΔS/N[g]	ΔSNS[h] (%)
	SC[b]	NC[c]	SW[d]	NW[e]			
Control	42.23 mm d^{-1}	22.40 mm d^{-1}	40.71 mm d^{-1}	23.57 mm d^{-1}	2.74(100%)	2.95(100%)	1.73(100%)
Middle Topography	−15.92	−9.64	−11.59	6.60	−0.52(−18.98)	−0.37(−12.54)	−23.56
Low Topography	−26.42	−10.35	−91.54	9.03	−0.75(−27.37)	−1.72(−58.31)	−35.12
Large Paratethys	−6.05	−5.69	−15.52	27.16	−0.71(−25.91)	−0.58(−19.66)	6.71
Middle Paratethys	−6.40	−20.04	−15.85	36.07	−0.95(−34.67)	−0.54(−18.31)	−2.61
Small Paratethys	−4.14	1.24	0	5.50	−0.20(−7.30)	−0.16(−5.42)	2.94
Absent Indian Peninsular	12.37	2.45	−3.65	25.16	−0.36(−13.14)	−0.25(−8.47)	−62.33
Small South China Sea	−24.52	−7.43	−12.07	8.03	−0.68(−24.82)	−0.56(−18.98)	12.37
Absent South China Sea	−42.11	−8.24	−16.32	7.17	−0.96(−35.04)	−0.86(−29.15)	−13.14
Small East China Sea	−0.87	−12.72	−0.58	−1.50	−0.10(−3.65)	0.20(6.78)	−2.21
Absent East China Sea	−9.33	−32.80	0	−0.24	−0.47(−17.15)	0.40(13.56)	1.76
Scenario I	−54.64	−30.59	−77.55	79.27	−1.92(−70.07)	−2.15(−72.88)	−31.06
Scenario II	−58.11	−35.51	−25.84	19.87	−1.60(−58.39)	−1.12(−37.96)	−37.11
Scenario III	−9.52	−1.56	−12.11	5.15	−0.31(−11.31)	−0.37(−12.54)	−2.21

[a] ΔP: the regional precipitation changes in percentages compared with the control run. All ΔPs reported here are calculated from the points in which the changes of precipitation compared to the control run passes 95% confidence level.
[b] SC: the Yangtze River valley and the area south of it (22°–30°N, 105°–120°E) comprise 12 points in the IAP-AGCM model.
[c] NC: the Yellow River valley (34°–42°N, 105°–120°E) comprises 12 points in the model.
[d] SW: Himalaya and South Tibet (26°–30°N, 80°–100°E) comprises 10 points in the model.
[e] NW: North Tibet and Central Asia (34°–46°N, 75°–100°E) comprises 24 points in the model.
[f] M/I: ((precipitation in SC+precipitation in NC)/24)/(precipitation in NW/24). ΔM/I: the changes of the rations, with percentages in brackets.
[g] S/N: ((precipitation in SC+precipitation in SW)/22)/((precipitation in NC+precipitation in NW)/36). ΔS/N: the changes of the rations, with percentages in brackets.
[h] SNS: wind seasonality in East China (including SC and NC together). ΔSNS: the changes of SNS value in percentages.

valley and the area south of it, the Yellow River valley and North Tibet and Central Asia. No significant variations are observed for Himalaya and South Tibet. These precipitation anomalies lead to a 0.47 decrease in M/I and a 0.40 increase in S/N (Table 1), indicating that the East China Sea transgression mainly intensifies the east–west aridity/humidity contrasts and has a negligible role in the magnification of the south–north contrasts.

5. Evolution of climate pattern in scenario experiments

5.1. Evolution of precipitation

Great changes of precipitation fields are observed in the three scenario experiments (Fig. 4a to c). The zonal deficient rain band with precipitation less than 1.5 mm/d is wide, and latitudinally controls almost whole China in the Scenario I. The first stage of paleogeographic evolution considerably increases precipitation over Himalaya and South Tibet. The deficient rain band becomes narrower and inclined from the southeast to the northwest, and the south–north aridity/humidity contrasts are magnified in the Scenario II. The second stage of paleogeographic evolution markedly increases the precipitation over East China. The deficient rain band is located over North Tibet and Central Asia. The east–west aridity/humidity contrasts are intensified in the Scenario III.

5.2. Evolution of wind seasonality

Corresponding to the above changes in precipitation fields, the areas with SNS values greater than 2 gradually extend northward over East China (Fig. 4e to f), indicating the spatial development of monsoon regions. The SNS structures similar to the control run form later over East China than over South Asia. The large-SNS cell moves to the Indian Peninsular earlier in the first stage of paleogeographic reconstruction, while the SNS pattern in China similar to the control run occurs in the second stage. This sequence suggests that the intensification of monsoon over South Asia should be earlier than that over East China.

5.3. Evolution of atmospheric dynamics

The paleogeographic evolution also leads to the large-scale reorganizations of pressure structure (Fig. 5). In summer, the low-pressure cell, originally located over China in the Scenario I, moves to the Indian peninsular in the Scenario II and then is deepened in the Scenario III.

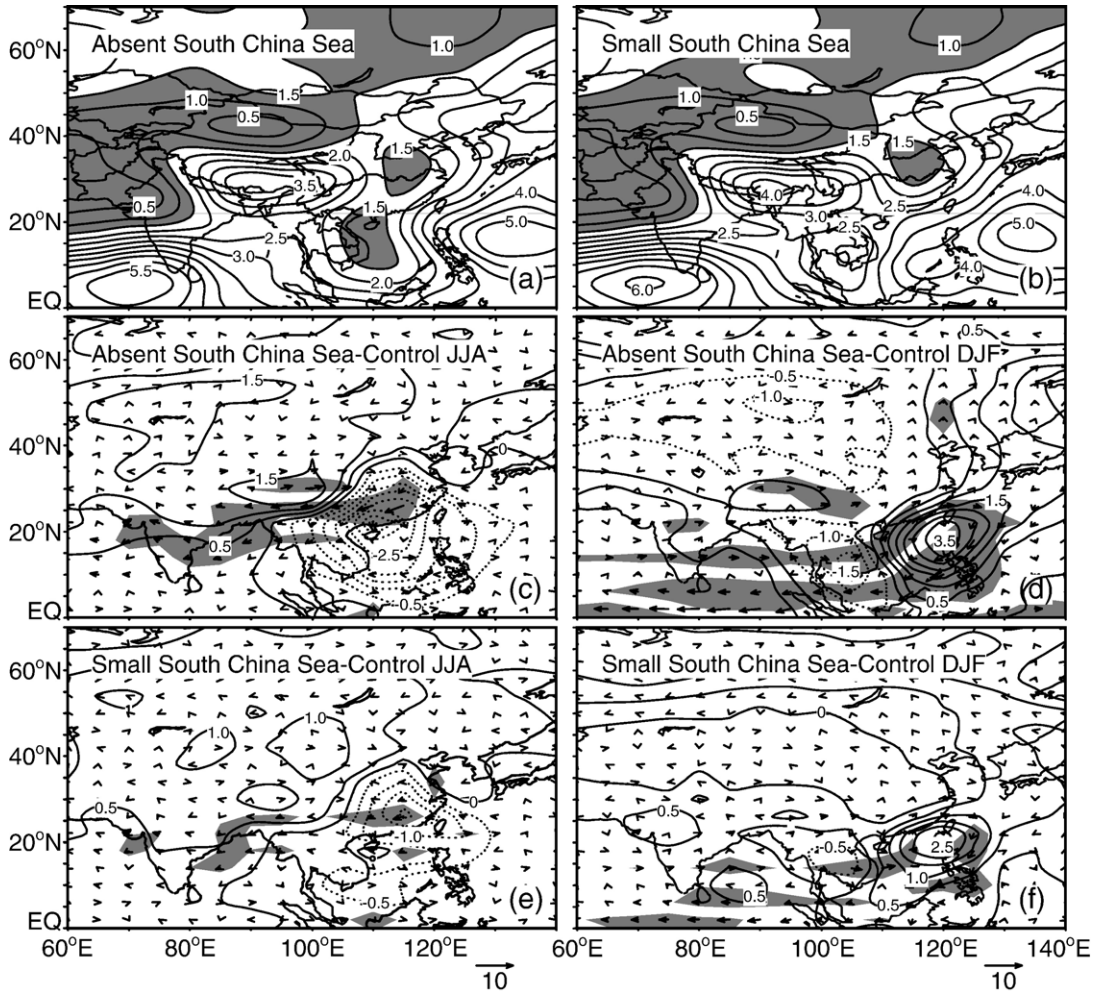

Fig. 3. The impacts of the South China Sea forcing on the precipitation (mm/d), sea level pressure (hPa) and the 850 hPa winds, (a) for the precipitation fields simulated in the absent South China Sea experiment, (b) for the precipitation fields in the small South China Sea experiment, (c) and (d) for the pressure structure and the wind anomalies between the absent South China Sea experiment and the control respectively in summer (JJA) and winter (DJF), (e) and (f) for the pressure structure and the wind anomalies between the small South China Sea experiment and the control respectively in summer and winter. The areas with precipitation less than 1.5 mm/d are shaded in the (a) and (b), and the areas within the 95% confidence level of the 850 hPa wind anomalies are shaded in the (c) to (f).

The changes of the low-pressure cell strengthen the westerlies/southwesterlies over Asia. The high-pressure cell, which is originally located over the Paratethys, gradually diminishes during the shrinkage of the sea. As a result, the anomalous cyclonic circulations considerably strengthen the southwesterlies over East Asia (e.g., [19]).

In the first stage of paleogeographic evolution, the reorganizations of pressure structure in summer cause the strong anomalies in the westerlies over the Arabian Sea and South Asia, but only lead to minor winds anomalies over East China (Fig. 5e). Significant anomalies in the southwesterlies over East China emerge later (Fig. 5f) in the second stage. These changes in 850 hPa winds are consistent well with the SNS results.

6. Functional comparison of forcing factors

The magnification of the south–north aridity/humidity contrasts in the first stage of paleogeographic evolution relates to the following five changes of lower boundary conditions: 1) the topography uplift from the low range to the middle one, 2) the Paratethys retreat from the large size to the middle extension, 3) the South China Sea expansion from the land to the small sea, 4) the East China Sea transgression to the small state and 5) the Indian peninsular drift to the present situation. Among these five factors, greatest impacts on the S/N are observed for the topography uplift (Fig. 6a). Furthermore, the first stage of paleogeographic evolution causes the markedly

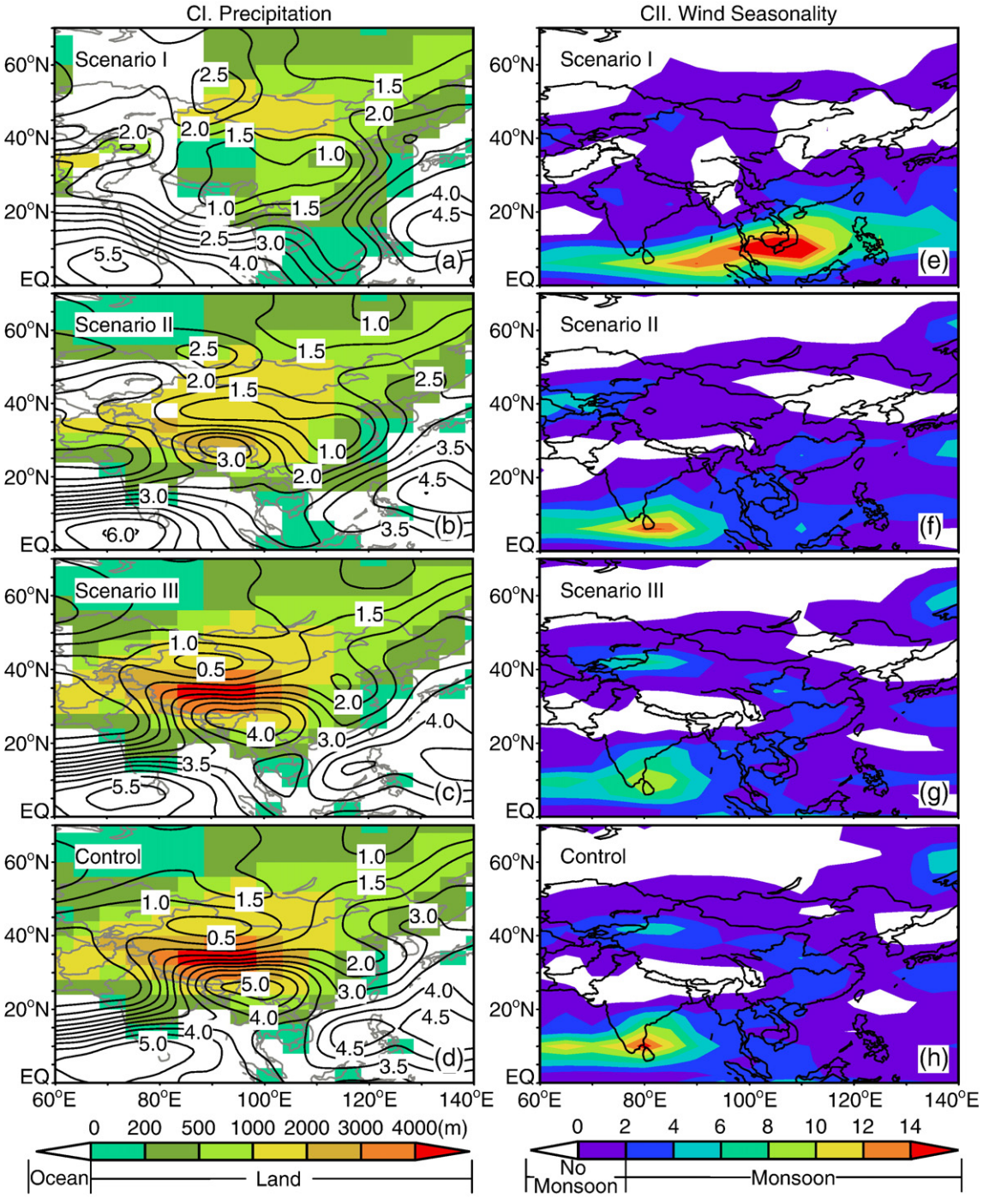

Fig. 4. The precipitation fields (left column CI, mm/d) and SNS fields (right column CII) in the scenario experiments and the control run. In the left column, the black lines are precipitation isohyets (mm/d) and the color blocks represent the topography and land–sea distribution. In the right column, the SNS values are shown in color scales.

increased precipitation over Himalaya and South Tibet, where the impact of topographic changes is the most important (Fig. 6b). Our results therefore indicate that the topography rising (mainly uplift of the Himalaya–Tibetan plateau) plays the primary role in the magnification of the south–north aridity/humidity contrasts.

The formation of the east–west aridity/humidity contrasts in the second stage appears to be linked with

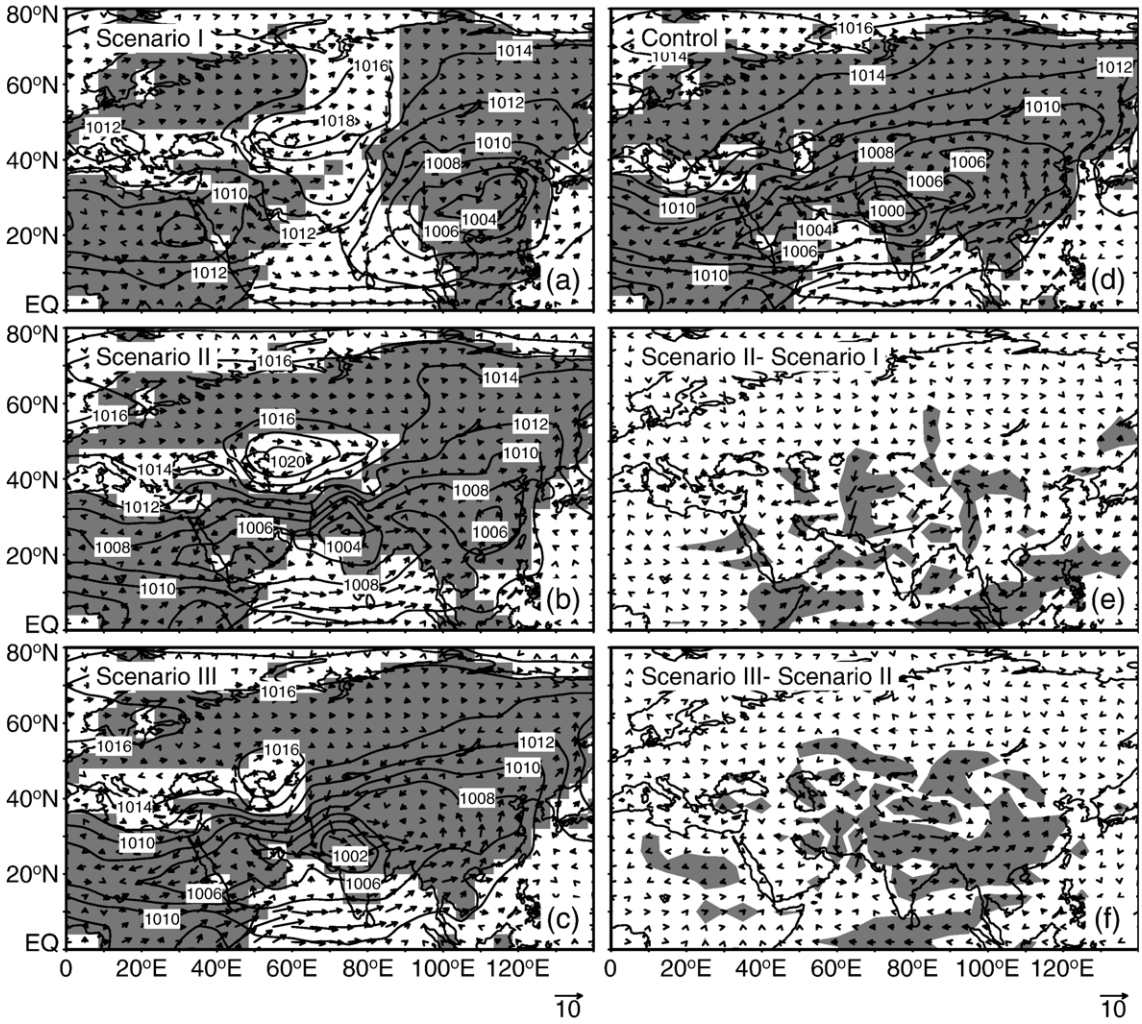

Fig. 5. Sea level pressure (hPa) and wind fields at 850 hPa (m/s), (a) for the Scenario I, (b) for the Scenario II, (c) for the Scenario III, (d) for the control run, (e) for the wind anomalies between the Scenario II and the Scenario I and (f) for the wind anomalies between the Scenario III and the Scenario II. The land areas are shaded in the (a) to (d). The areas within the 95% confidence level are shaded in the (e) and (f).

the following four changes of lower boundary conditions: 1) the increased topography from the middle elevation to the present height, 2) the shrinkage of the Paratethys from the middle extension to the small one, 3) the further expansion of the South China Sea to the current size and 4) the transgression of the East China Sea to the present state. Our simulations suggest the negligible impacts of East China Sea transgression (Fig. 6c). Moreover, no large-scale East China Sea transgression occurs near the Oligocene/Miocene boundary [49]. The Paratethys retreat, the South China Sea expansion and the Himalaya–Tibetan plateau uplift play important roles in the formation of the east–west aridity/humidity contrasts. The changes in M/I ratios reveal that the Paratethys retreat is the most important forcing, then the South China Sea expansion and last the Himalaya–Tibetan plateau uplift.

The above ranking of importance is also supported by the comparison among the Scenario II, the Scenario III, the middle Paratethys, the small Paratethys and the six supplementary experiments (Supplementary materials). The experiments with the middle Paratethys condition produce much lower M/I ratios than the control run, regardless the changes of the other three factors (South China Sea, topography and East China Sea). In the experiments, where the Paratethys and the South China Sea are both kept at small sizes, the planetary-wave-dominant patterns with the low M/I ratios are maintained, despite the changes of the latter two factors (topography and East China Sea). However, the experiments show the

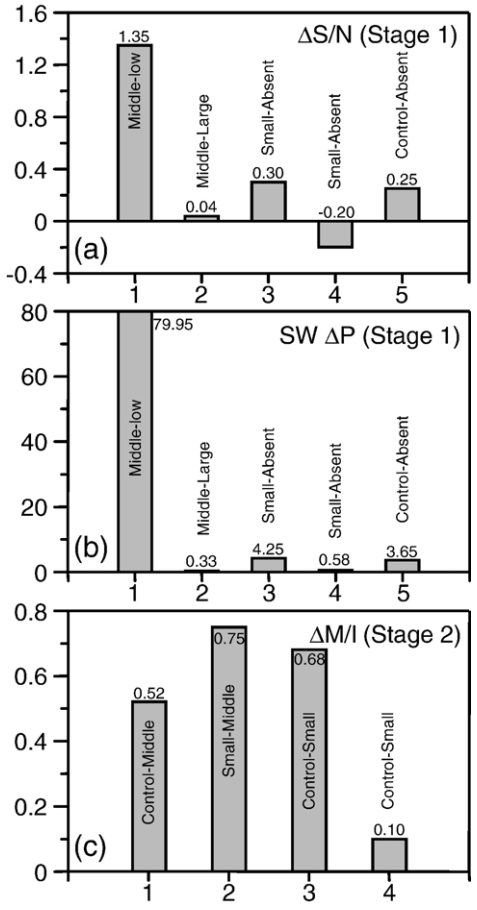

Fig. 6. Functional comparison of the forcing factors, (a) the changes in S/N ratios induced by the forcing factors in the first stage of paleogeographic evolution, (b) the precipitation changes (%) in Himalaya and South Tibet made by the forcing factors in the first stage, (c) the variations of M/I ratios led by the forcing factors in the second stage. In the horizontal scale, 1 represents the Himalaya–Tibetan plateau uplift, 2 the Paratethys retreat, 3 the South China Sea expansion, 4 the East China Sea transgression and 5 the Indian peninsular drift. For example, the first bar from the left in (a) shows that the Himalaya–Tibetan plateau uplift from the low condition to the middle range causes an increased S/N of 1.35.

monsoon climate with the higher M/I ratios close to the control run, when the Paratethys is kept at the small size, the South China Sea is expanded to the present size and the topography is risen to the current height.

7. Discussions

Our earlier studies [18,19] have revealed that the deficient rain bands with precipitation less than 1.5 mm/d in the simulations by the IAP-AGCM can be regarded as arid/semiarid regions. Thus, the above changes of precipitation patterns in the three scenario experiments quantitatively reconstruct the Cenozoic paleoclimatic evolution in China.

Our simulations illustrate that the intensified monsoon circulations and the abundant presence of water vapor are the two necessary conditions for the monsoon-dominant climate in China. Earlier studies [11–19] and the analyses here reveal that the Paratethys retreat and the Himalaya–Tibetan plateau uplift strengthen the monsoon circulations to provide the dynamic condition for the paleoclimatic evolution in China. Furthermore, our study clearly demonstrates that the South China Sea expansion is also an indispensable forcing for the monsoon-dominant climate in China. The later factor provides sufficient water vapor for the summer precipitation over East China. Otherwise, East China would be arid, even the Paratethys and the Himalaya–Tibetan plateau reach the present status and cause the strong summer winds that are comparable to the present state (Fig. 4). The modern observations [9] also demonstrate that the South China Sea, with the area about 3,500,000 km^2, is the most important water vapor source for monsoon precipitation in China. The ratio of water vapor fluxes from the South China Sea, the Bay of Bengal and the ocean located on the southeast of China is estimated to be 691:1:0.34 [9].

Geologic reconstructions [4–6] have brought forth the hypothesis that East Asian monsoon climate may have formed in the Late Oligocene. The hypothesis is also attested by the Qin An loess–paleosol sequences [59], the fine grained sediments [60,61] contributed by loess [62] in Lin Xia Basin and the evidence from the South China Sea [20]. Our simulations offer a new clue to examine the hypothesis. The Paratethys retreat to the Turan plate, the South China Sea larger than 2/5 of present state and the Himalaya–Tibetan plateau averagely higher than 1500 m are suggested to be the sufficient condition for the onset of the monsoon climate in China. The sufficient condition will be helpful to judge whether the monsoon climate has been formed in the Late Oligocene, provided that geologic research gives the state of the Paratethys, the size of the South China Sea and the height of the Himalaya–Tibetan plateau at that time.

With the three scenario experiments, our simulations highlight the general picture of Asian monsoon evolution during the Cenozoic. Tropical monsoon dominates the Indochina Peninsular in the Paleocene. The basic structure of the Asian monsoon system is established in the Eocene/Oligocene, but the monsoon at that time is still too weak to change the basic climatic pattern in China. In the Neogene, the markedly intensified monsoon circulations, which are strong

enough to extend to Yellow River valley, and the sufficient water vapor, cause the onset of monsoon climate in China. The above picture suggests an earlier initial form of the monsoon over South Asia, but needs to be tested by geologic records.

The other two factors newly addressed in our study, the Indian Peninsular drift and the East China Sea transgression, have weak impacts on Chinese paleoclimatic evolution. But the Indian Peninsular drift is able to change the land–sea thermal contrasts and deepen the monsoon low pressure to strengthen the westerlies over South Asia in summer. The impacts of the East China Sea transgression potentially may be magnified or dampened by the ocean feedback processes that are not addressed here.

Our study is still limited by the coarse resolution of the IAP-AGCM, though we think that the coarse resolution will not affect the here presented reconstructions of the basic climatic patterns in China. The new factors (the Indian Peninsular and the South China Sea) that include 25 and 16 grid points can substantially impact the climate in the model. The fixed SSTs also limit us to consider feedbacks involving changes in the ocean. It still remains a task to compare our study with the future experiments that are based on the similar scenarios and carried by models with high-resolution or coupled models.

In summary, our simulations demonstrate again that the Cenozoic paleogeographic evolution drives the reorganization of the paleoclimatic patterns in China. Our results suggest that the South China Sea expansion is another indispensable forcing that provides water vapor condition for the monsoon-dominant climate in China, in addition to the Himalaya–Tibetan plateau uplift and the Paratethys retreat that strengthen the atmospheric dynamic condition. The coaction of these three factors causes the monsoon-dominant climate with the remarkable east–west aridity/humidity contrasts in China. Our simulations also suggest a possible earlier inception of monsoon over South Asia than over East Asia.

Acknowledgments

This study is jointly supported by the National Natural Science Foundation of China (Grant No. 40631005, 40221503), the Key Program of Chinese Academy of Sciences (Grant No. KZCX2-YW-117) and the China Postdoctoral Science Foundation. We wish to thank Lixia Ju, Yali Zhu and Linling Chen for help in the revision, Ingo Bethke and Misha Bowles for improving the English, W. F. Ruddiman, two anonymous reviewers and M.L. Delaney for the constructive reviews and suggestions.

Appendix A. Supplementary data

Supplementary data associated with this article can be found, in the online version, at doi:10.1016/j.epsl.2007.03.024.

References

[1] G.H. Wu, L.S. Tian, S.X. Hu, N.A. Wang (Eds.), Physical Geography, third, Higher Education Press, Beijing, 2000, (in Chinese).
[2] T.R. Zhou, Palaeogeography, Beijing Normal University Press, Beijing, 1982 (in Chinese).
[3] P.X. Wang, Neogene stratigraphy and paleoenvironments of China, Palaeogeogr. Palaeoclimatol. Palaeoecol. (77) (1990) 315–334.
[4] T.S. Liu, Z.T. Guo, Geological environment in China and global Change, in: Z.S. An (Ed.), Selected Works of Liu Tungsheng, Science Press, Beijing, 1997, pp. 192–202.
[5] X.J. Sun, P.X. Wang, How old is the Asian monsoon system? — Palaeobotanical records from China, Palaeogeogr. Palaeoclimatol. Palaeoecol. (222) (2005) 181–222.
[6] Z.S. Zhang, Z.T. Guo, Spatial character reconstruction of different periods in Oligocene and Miocene, Quat. Sci. 25 (4) (2005) 523–530 (in Chinese with English abstract).
[7] E. Halley, An historical account of the trade winds and monsoons observable in the seas between and near the tropics with an attempt to assign the physical cause of the said wind, Philos. Trans. R. Soc. Lond. 16 (1686) 153–168.
[8] H. Flöhn, Der indische sommermonsun als Glied der planetarischen Zirkulation der atmosphere, Bec. Des D. wd. Bd., vol. 4, 1956, p. 22.
[9] L.X. Chen, Q.G. Zhu, H.B. Luo, J.H. He, M. Dong, Z.Q. Feng, The East Asian Monsoon, China Meteorological Press, 1991 (in Chinese).
[10] S. Manabe, T.B. Terpstra, The effects of mountains on the general circulation of the atmosphere as identified by numerical experiments, J. Atmos. Sci. 31 (1974) 3–42.
[11] W.F. Ruddiman, J.E. Kutzbach, Forcing of Late Cenozoic northern hemisphere climate by plateau uplift in Southern Asia and the American West, J. Geophys. Res. 94 (1989) 18409–18427.
[12] W.L. Prell, J.E. Kutzbach, Sensitivity of the Indian monsoon to forcing parameters and implications for its evolution, Nature 360 (1992) 647–652.
[13] Z.S. An, J.E. Kutzbach, W.L. Prell, S.C. Porter, Evolution of Asian monsoons and phased uplift of the Himalaya–Tibetan plateau since Late Miocene times, Nature 411 (2001) 62–66.
[14] X.D. Liu, Z.Y. Yin, Sensitivity of East Asian monsoon climate to the uplift of the Tibetan Plateau, Palaeogeogr. Palaeoclimatol. Palaeoecol. (183) (2002) 223–245.
[15] A. Kitoh, Effects of mountain uplift on East Asian summer climate investigated by a coupled atmosphere–ocean GCM, J. Clim. 17 (4) (2004) 783–802.
[16] G. Ramstein, F. Fluteau, J. Besse, S. Joussaume, Effect of orogeny, plate motion and land–sea distribution on Eurasian climate change over the past 30 million years, Nature 386 (1997) 788–795.
[17] F. Fluteau, G. Ramstein, J. Besse, Simulating the evolution of the Asian and African monsoons during the past 30 Myr using an atmospheric general circulation model, J. Geophys. Res. 104 (1999) 11995–12018.

[18] Z.S. Zhang, H.J. Wang, Z.T. Guo, D. Jiang, Impact of topography and land–sea distribution on East Asian paleoenvironmental patterns, Adv. Atmos. Sci. 23 (2006) 258–266.
[19] Z.S. Zhang, H.J. Wang, Z.T. Guo, D. Jiang, What triggers the transition of palaeoenvironmental patterns in China, the Tibetan Plateau uplift or the Paratethys Sea retreat? Palaeogeogr. Palaeoclimatol. Palaeoecol. (2007) 317–331, doi:10.1016/j.palaeo.2006.08.003.
[20] P. Wang, Z. Jian, Q. Zhao, Q. Li, R. Wang, Z. Liu, G. Wu, L. Shao, J. Wang, B. Huang, D. Fang, J. Tian, J. Li, X. Li, G. Wei, X. Sun, Y. Luo, X. Su, S. Mao, M. Chen, Evolution of the South China Sea and monsoon history revealed in deep-sea records, Chin. Sci. Bull. 48 (2003) 2549–2561.
[21] J.J. Li, Z.J. Zhao, Morden theoretical significance of "the dry pole of Asia" by P. Teilhard de Chardin, Quat. Sci. 23 (2003) 366–371 (in Chinese with English abstract).
[22] X.Q. Bi, IAP 9-level atmospheric general circulation model and climate simulation, PhD Thesis, Institute of Atmosphere Physics, Chinese Academy of Sciences, Beijing, 1993 (in Chinese with English abstract).
[23] D. Jiang, H.J. Wang, Z.L. Ding, X. Lang, H. Drange, Modeling the middle Pliocene climate with a global atmospheric general circulation model, J. Geophys. Res. 110 (2005), doi:10.1029/2004JD005639.
[24] D. Jiang, H.J. Wang, H. Drange, X. Lang, Last glacial maximum over China: Sensitivities of climate to palaeovegetation and Tibetan ice sheet, J. Geophys. Res. 108 (2003), doi:10.1029/2002JD002167.
[25] L. Ju, H.J. Wang, D. Jiang, Simulation of the Last Glacial Maximum climate over East Asia with a regional climate model nested in a general circulation model, Palaeogeogr. Palaeoclimatol. Palaeoecol. (in press), doi:10.1016/j.palaeo.2006.12.012.
[26] J.F. Wei, H.J. Wang, A possible role of solar radiation and ocean in the Mid-Holocene East Asian monsoon climate, Adv. Atmos. Sci. 21 (2004) 1–12.
[27] X.H. Zhang, Dynamical framework of IAP nine-level atmospheric general circulation model, Adv. Atmos. Sci. 7 (1990) 66–77.
[28] X.Z. Liang, Description of a nine-level Atmospheric General Circulation Model, Adv. Atmos. Sci. 13 (1996) 269–298.
[29] X.C. Jin, Z.Y. Zhou, P.X. Wang, Ocean Drilling and Earth Sciences in China, Tongji University Press, Shanghai, 1995 (in Chinese).
[30] T.H. Andel, New Views on an Old Planet, Cambridge University Press, 1985.
[31] A. Yin, T.M. Harrison, Geologic evolution of the Himalayan–Tibetan orogen, Annu. Rev. Earth Planet. Sci. 28 (2000) 211–280, doi:10.1146/annurev.earth.28.1.211.
[32] P. Tapponnier, Z. Xu, F. Roger, B. Meyer, N. Arnaud, G. Wittlinger, J. Yang, Oblique stepwise rise and growth of the Tibet Plateau, Science 294 (2001) 1671–1677.
[33] A. Briais, P. Patriat, P. Tapponnier, Updated interpretation of magnetic anomalies and seafloor spreading stages in the South China Sea: Implications for the Tertiary tectonics of Southeast Asia, J. Geophys. Res. 98 (B4) (1993) 6299–6328.
[34] M.A. Akhmet'ev, G.N. Aleksandrova, E.O. Amon, V.N. Beniamovskii, E.M. Bugrova, O.N. Vasil'eva, Z.I. Glezer, V.I. Zhelezko, N.I. Zaporozhets, G.E. Kozlova, I.A. Nikolaeva, T.V. Oreshkina, L.A. Panova, E.P. Radionova, N.I. Strel'nikova, A.I. Yakovleva, Biostratigraphy of the marine Paleogene in the West Siberian plate, Stratigr. Geol. Corre. 9 (2) (2001) 132–158.
[35] T.M. Harrison, P. Copeland, W.S.F. Kidd, A. Yin, Raising Tibet, Science 255 (1992) 1663–1670.
[36] R. Xu, Vegetational changes in the past and the uplift of Qinghai–Xizang Plateau, Geological and ecological studies of Qinghai–Xizang Plateau, vol. V1, Science Press, Beijing, 1981, pp. 139–148.
[37] X.Y. Sun, Y.N. Zhao, Z.S. He, The Oligocene–Miocene palynological assemblages from the Xining–Minghe basin, Qinghai Province, Geol. Rev. 30 (3) (1984) 207–216 (in Chinese with English abstract).
[38] L.Y. Tang, C.M. Shen, Late Cenozoic vegetational history and climatic characteristic of Qinghai–Xizang Plateau, Acta Micropalaeont. Sin. 13 (4) (1996) 321–337 (in Chinese with English abstract).
[39] Y.F. Shi, M.C. Tang, Y.Z. Ma, Linkage between the second uplifting of the Qinghai–Xizang (Tibetan) Plateau and the initiation of the Asian monsoon system, Sci. China, Ser. D: Earth Sci. 42 (1999) 303–312.
[40] Z.D. Qiu, C.K. Li, Evolution of Chinese mammalian fauna and Tibetan Plateau uplift, Sci. China, Ser. D: Earth Sci. 34 (2004) 845–854 (in Chinese).
[41] X. Wang, Z.X. Qiu, B.Y. Wang, Hyaenodonts and carnivorans from the early Oligocene to early Miocene of Xianshuihe Formation, Lanzhou Basin, Gansu Province, China, in: C. Badgley, L.J. Flynn, L.L. Jacobs, L.H. Taylor (Eds.), Paleontology from China, Pakistan and Around the World in Honor of Will Downs, Palaeotologia Electronica, vol. 8(1.6A), 2005, pp. 1–14.
[42] C.N. Garzione, D.L. Dettman, J. Quade, P.G. DeCelles, R.F. Butler, High times on the Tibetan Plateau: Paleoelevation of the Thakkhola Graben, Nepal, Geology 28 (2000) 339–342.
[43] D.B. Rowley, R.T. Pierrehumbert, B.S. Currie, A new approach to stable isotope-based paleoaltimetry: Implications for paleoaltimetry and paleohypsometry of the High Himalaya since the Late Miocene, Earth Planet, Sci. Lett. 188 (2001) 253–268.
[44] R.A. Splcer, N.B. Harris, M. Widdowson, A.B. Herman, S. Guo, P.J. Valdes, J.A. Wolfe, S.P. Kelley, Constant elevation of southern Tibet over the past 15 million years, Nature 421 (2003) 622–624.
[45] D.B. Rowley, B.S. Currie, Palaeo-altimetry of the late Eocene to Miocene Lunpola basin, central Tibet, Nature 439 (2006) 677–681, doi:10.1038/nature04506.
[46] J. Dercourt, L.E. Ricou, B. Vrielinck (Eds.), Atlas Tethys Palaeoenvironmental Maps, Gauthier-Villars, Paris, 1993.
[47] F. Rögl, Palaeogeographic considerations for Mediterranean and Paratethys seaways (Oligocene to Miocene), Ann. Naturhist. Mus. Wien 99A (1998) 279–310.
[48] M. Harzhauser, W.E. Piller, F.F. Steininger, Circum-Mediterranean Oligo-Miocene biogeographic evolution — The gastropods' point of view, Palaeogeogr. Palaeoclimatol. Palaeoecol. (183) (2002) 103–133.
[49] Y.H. Chen, Cretaceous–Tertiary palaeogeography of the East China Sea, Acta Sedimentol. Sin. 7 (4) (1989) 69–76 (in Chinese with English abstract).
[50] J. Zachos, M. Pagani, L. Sloan, E. Thomas, K. Billups, Trends, rhythms, and aberrations in global climate 65 Ma to present, Science 292 (2001) 686–693.
[51] M. Kathryn, B. Jan, B. Henk, C.C. Steven, C. Thomas, R.D. Gerald, E. Frédérique, G. Jérôme, J. Martin, W.J. Richard, K. Michael, K. John, K. Nalan, K. Alexey, M. Nahysa, M. Jens, M. David, C.M. Theodore, O. Jonaotaro, O.R. Matthew, P. Heiko, R. Brice, R. Domenico, S. Tatsuhiko, C.S. David, S. Ruediger, S.J. Kristen, S. Itsuki, S. Noritoshi, T. Kozo, W. Mahito, Y. Masanobu, F. John, F. Martin, K. Peter, J. Wilfried, K. Yngve, The Cenozoic palaeoenvironment of the Arctic Ocean, Nature 441 (2006) 601–605, doi:10.1038/nature04800.
[52] M.A. Cane, P. Molnar, Closing of the Indonesian seaway as a precursor to east African aridification around 3–4 million years ago, Nature 411 (2001) 157–162.

[53] J. Quade, T.E. Cerling, J.R. Bowman, Development of Asian monsoon revealed by marked ecological shift during the latest Miocene in northern Pakistan, Nature 342 (1989) 163–166.
[54] T.E. Cerling, J.M. Harris, B.J. MacFadden, M.G. Leakey, J. Quade, V. Eisenmann, J.R. Ehleringer, Global vegetation change through the Miocene/Pliocene boundary, Nature 389 (1997) 153–158.
[55] C.D. Keeling, T.P. Whorf, Atmospheric CO2 records from sites in the SIO air sampling network, in Trends: A Compendium of Data on Global Change, Carbon Dioxide Information Analysis Center, Oak Ridge National Laboratory, U.S. Department of Energy, Oak Ridge, Tenn., 2003, http://cdiac.esd.ornl.gov/trends/co2/sio-mlo.htm.
[56] H.J. Dowsett, J.A. Barron, R.Z. Poore, R.S. Thompson, T.M. Cronin, S.E. Ishman, D.A. Willard, Middle Pliocene paleoenvironmental reconstruction: PRISM2, U.S. Geological Survey Open File Report, 1999, pp. 99–535.
[57] Q.C. Zeng, B.L. Zhang, On the seasonal variation of atmospheric general circulation and the monsoon, Chin. J. Atmos. Sci. 22 (1998) 211–220.
[58] J.P. Li, Q.C. Zeng, A new monsoon index and the geographical distribution of the global monsoon, Adv. Atmos. Sci. 20 (2003) 299–302.
[59] Z.T. Guo, W.F. Ruddiman, Q.Z. Hao, H.B. Wu, Y.S. Qiao, R.X. Zhu, S.Z. Peng, J.J. Wei, B.Y. Yuan, T.S. Liu, Onset of Asian Desertification by 22 Ma ago inferred from loess deposits in China, Nature 416 (2002) 159–163.
[60] J.J. Li, X.M. Fang, Uplift of the Tibetan Plateau and environmental changes, Chin. Sci. Bull. 44 (1999) 2117–2124.
[61] X. Fang, C.N. Garzione, R. Van der Voo, J. Li, M. Fan, Flexural subsidence by 29 Ma on the NE edge of Tibet from the magnetostratigraphy of Linxia basin, China, Earth and Planet, Sci. Lett. 210 (2003) 545–560.
[62] C.N. Garzione, J.I. Matt, R.B. Asish, Source of Oligocene to Pliocene sedimentary rocks in the Linxia basin in northeastern Tibet from Nd isotopes: Implications for tectonic forcing of climate, Geol. Soc. Amer. Bull. 117 (2005) 1156–1166.